Nanoscale Res Lett (2010) 5:935–940
DOI 10.1007/s11671-010-9582-5

NANO EXPRESS

Berkovich Nanoindentation on AlN Thin Films

Sheng-Rui Jian · Guo-Ju Chen · Ting-Chun Lin

Received: 6 January 2010 / Accepted: 16 March 2010 / Published online: 31 March 2010

Abstract Berkovich nanoindentation-induced mechanical deformation mechanisms of AlN thin films have been investigated by using atomic force microscopy (AFM) and cross-sectional transmission electron microscopy (XTEM) techniques. AlN thin films are deposited on the metal-organic chemical-vapor deposition (MOCVD) derived Si-doped (2×10^{17} cm^{-3}) GaN template by using the helicon sputtering system. The XTEM samples were prepared by means of focused ion beam (FIB) milling to accurately position the cross-section of the nanoindented area. The hardness and Young's modulus of AlN thin films were measured by a Berkovich nanoindenter operated with the continuous contact stiffness measurements (CSM) option. The obtained values of the hardness and Young's modulus are 22 and 332 GPa, respectively. The XTEM images taken in the vicinity regions just underneath the indenter tip revealed that the multiple "pop-ins" observed in the load–displacement curve during loading are due primarily to the activities of dislocation nucleation and propagation. The absence of discontinuities in the unloading segments of load–displacement curve suggests that no pressure-induced phase transition was involved. Results obtained in this study may also have technological implications for estimating possible mechanical damages induced by the fabrication processes of making the AlN-based devices.

Keywords AlN · Nanoindentation · Focused ion beam · Transmission electron microscopy

S.-R. Jian (✉) · G.-J. Chen · T.-C. Lin
Department of Materials Science and Engineering, I-Shou University, Kaohsiung 840, Taiwan, ROC
e-mail: srjian@gmail.com

Introduction

The advent and development of microsystems and nanotechnology has its roots in surface and materials science, and in particular, thin films. In the past, many such materials have only been characterized in terms of their electronic, magnetic, and optical properties. Nevertheless, their mechanical and structural characteristics are now just as important. This is because traditional methods such as bulge and tensile testing are impractical and/or unsuitable, since they do not scale well into the micro- and nanoscale. Recently, it has become clear that, in order to fully harvest the unprecedented potential of the emerging nanotechnologies in general, the processes-induced structural and mechanical modifications on the materials might be equally important. For instance, during the past decade, AlN has emerged as an active photonic material for applications in deep ultraviolet emitters and detectors due to its large direct bandgap of 6.2 eV [1, 2]. It has strong chemical bonds, making it highly stable and resistant to degradation as operating under harsh environments/conditions. Because of its high thermal conductivity, large piezoelectronic field, and low electron affinity, AlN also has applications in stable X-ray production, surface acoustic wave devices, and electron emission devices [3–5]. However, the successful fabrication of devices based on the epitaxial AlN thin films requires better understanding of the mechanical characteristics in addition to its electrical performances, since the contact loading during processing or packaging can significantly degrade the performance of these devices. Consequently, there is a growing demand of investigating the mechanical characteristics of materials, in particular in the nanoscale regime, for device applications.

This study addresses the nanoindentation analysis of the mechanical properties of AlN thin films. The nanoindentation technique is especially well suited for the characteristics of small structures [6–8] or thin films and coatings [9–12]. Analysis of the load–displacement curve obtained by nanoindentation permits mainly hardness and Young's modulus to be obtained without visualizing the indentation. The most usual method of analysis is the one proposed by Oliver and Pharr [13]. However, in the case of thin films, the response after some penetration depth is given not only by the films but also by the substrate and, the mechanical properties obtained are a combination of the true values of the films and the structure. Indentation with contact depths of less than 10% of films thickness is needed to obtain intrinsic film properties and avoid the influence of the substrate [14]. Besides, it is very difficult to obtain meaningful analytical results for indentation depths less than 10 nm because of the equipment limitations. Bearing in mind the above, it is obvious that it is not possible to obtain substrate-independent results for film less than 100 nm thick. Therefore, in order to analyze films less than 100 nm thick, it is essential to monitor the mechanical properties as a function of depth, in order to get an insight on the influence of the substrate. In this study, we use a dynamic approach, termed continuous stiffness measurement (CSM) mode [15], to continuously monitor the hardness and Young's modulus values as a function of the indentation depths.

While diamond anvil cell experiments are capable of investigating the mechanical and phase transformation in bulk materials under hydrostatic pressure [16], the materials behavior under nanoindentation is of more relevance to realistic contact loading conditions. However, the nanoindentation technique itself does not provide the information of subsurface indentation-induced deformation mechanisms and dislocation propagation. In this respect, the focused ion beam (FIB) miller is now widely used for preparing the cross-sections of the locally deformed areas to direct reflect the detailed nanoindentation-induced mechanical responses for a range of materials [17]. In our case here, the cross-sectional observations can provide important information about the in-depth phase distribution and the embedded defect features introduced by contact loading that were impossible to be observed with the plain-view samples.

Herein, in this study, the deformation behaviors of helicon sputtering method derived AlN thin films under contact loading have been investigated using Berkovich nanoindentation, followed by analysis using atomic force microscopy (AFM), FIB, and transmission electron microscopy (TEM) techniques, in order to understand the final structures of the indentation-induced transformation zones observed in experiments.

Experimental Details

Experimentally, AlN thin films used in this study were deposited on Si-doped (2×10^{17} cm^{-3}) GaN template, prepared by metal-organic chemical-vapor deposition (MOCVD) [18], using the helicon sputtering system which with an average thickness of about 400 nm. The detailed growth procedures of AlN thin films can be found elsewhere [19].

The mechanical properties of AlN thin films were characterized by means of an MTS NanoXP® (MTS Cooperation, Nano Instruments Innovation Center, TN, USA). The nanoindentation measurements, using a three-side pyramidal Berkovich diamond indenter of 40 nm radius (faces 65.3° from vertical axis), were conducted under the continuous stiffness measurement (CSM) procedures [15], which was accomplished by superimposing a small oscillation on the primary loading signal and analyzing the resulting response of the system by using a lock-in amplifier. Prior to real measurement, the indenter was loaded and unloaded three times to ensure that the tip was properly in contact with the surface of AlN thin films and that any parasitical phenomenon is released from the measurement. At the fourth time, the indenter was loaded at a strain rate of 0.05 s^{-1} until reaching an indent depth of 50 nm and was held for 10 s. Then, it was withdrawn with the same strain rate until 10% of the peak load was reached. At least 10 indents were performed on each sample. Each indentation was separated by 50 μm to avoid possible interferences between neighboring indents. We also followed the analytic method proposed by Oliver and Pharr [13] to determine the hardness and Young's modulus of AlN thin films from the load–displacement results. In this way, hardness and Young's modulus are obtained as a continuous function of penetration depth.

In addition, in order to reveal the role played by the nucleation and propagation of dislocations in indentation-induced deformation, cyclic nanoindentation tests were also performed in this study. These tests were carried out by the following sequences. First, the indenter was loaded to some chosen load and then unloaded by 90% of the previous load, which completed the first cycle. It then was reloaded to a larger chosen load and unloaded by 90% for the second cycle. Figure 2 illustrated a typical cyclic indentation test repeated for 2 cycles. It is noted that in each cycle, the indenter was hold for 30 s at 10% of its previous maximum load for thermal drift correction and for assuring that complete unloading was achieved. The thermal drift was kept below ± 0.05 nm/s for all indentations considered in this study. The same loading/unloading rate of 10 mN/s was used. At least 20 indents were performed on AlN thin films. The nanoindentations were sufficiently spaced to prevent from the mutual interactions.

The cross-sectional transmission electron microscopy (XTEM) samples were prepared from the indents by means of a dual-beam focused ion beam (FIB, Nova 220) station with Ga ions at 30 keV. Prior to milling, the FIB was used to deposit an ~1 μm thick layer of Pt to protect the AlN thin films surface. The details of FIB produces in preparing XTEM sample can be found elsewhere [17]. The XTEM lamella was examined in an FEI TECNAI G^2 TEM operating at 200 kV.

Results and Discussion

The typical load–displacement curve of AlN thin film obtained using the three-side pyramidal Berkovich diamond indenter is shown in Fig. 1. The total penetration depth into AlN thin film was ~58 nm with a peak load of 1 mN. And, the hardness and Young's modulus of AlN thin films were calculated from the load–displacement data followed the analytic method developed by Oliver and Pharr [13]. The hardness is estimated from

$$H = \frac{P_{\max}}{A_c}. \quad (1)$$

where $P_{\max}$ is the maximum indentation load and A_c is the projected contact area of the indentation. The projected area is determined from the indenter tip calibration and is a function of the contact depth (h_c). The contact depth is derived from the initial slope, $S = dP/dh$, of the first 50% of the last unloading curve and can be expressed as: $h_c = h_{\max} - \varepsilon(P_{\max}/S)$, where ε is the indenter constant (0.75 for a Berkovich indenter tip) and $h_{\max}$ is the total displacement under maximum indentation load. The stiffness, S, contains information of the modulus of the material, as following:

$$S = dP/dh = 2E_r\sqrt{\frac{A_c}{\pi}} \quad (2)$$

where E_r is the effective elastic modulus defined by

$$\frac{1}{E_r} = (1 - v_f^2)\frac{1}{E_f} + (1 - v_i^2)\frac{1}{E_i} \quad (3)$$

The elastic modulus E_i and Poisson's ratio v_i of the Berkovich indenter used in this study are 1141 GPa and 0.07 [13], respectively. As is commonly done, we assume that v_f is 0.25.

In addition, it is noted that the events of multiple pop-ins are coinciding nicely with sudden decreases in the hardness of measured materials [20]. The hardness of AlN thin film decreases abruptly at the penetration depth of ~12 nm corresponding to the first pop-in event, as shown in Fig. 2a. The hardness after the first pop-in for AlN thin film remains nearly constant at 22 GPa with small fluctuations, possibly associated with dislocation activities. Similarly, as shown in Fig. 2b), the Young's modulus of AlN films also displays a sudden drop occurring around the same penetration depth and then remains relatively constant at 332 GPa.

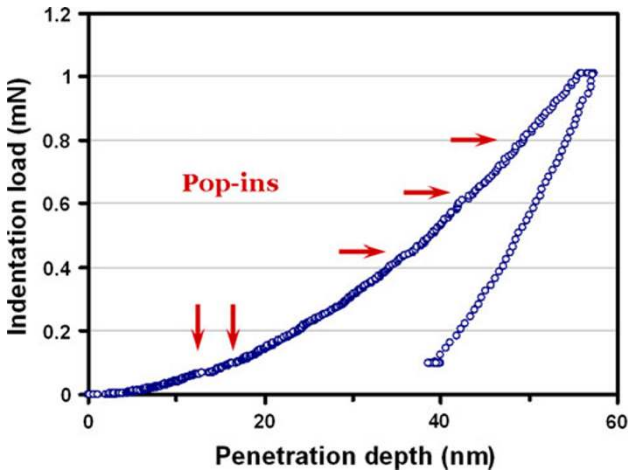

Fig. 1 The load–unloading curve displays the multiple pop-ins events (*arrows*) of AlN thin film

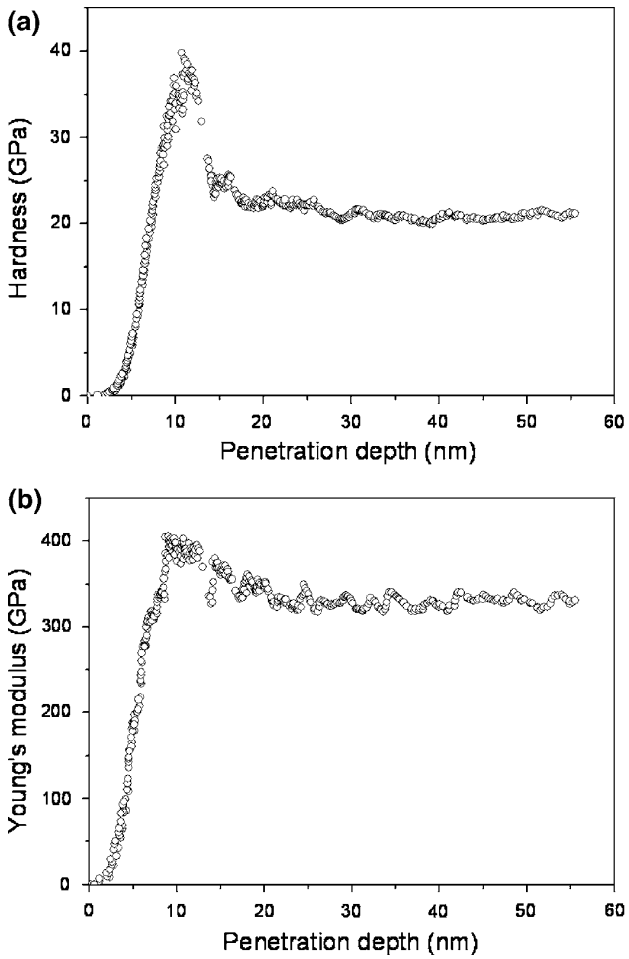

Fig. 2 Nanoindentation test results: (**a**) hardness–displacement curve and, (**c**) Young's modulus–displacement curve for AlN thin film

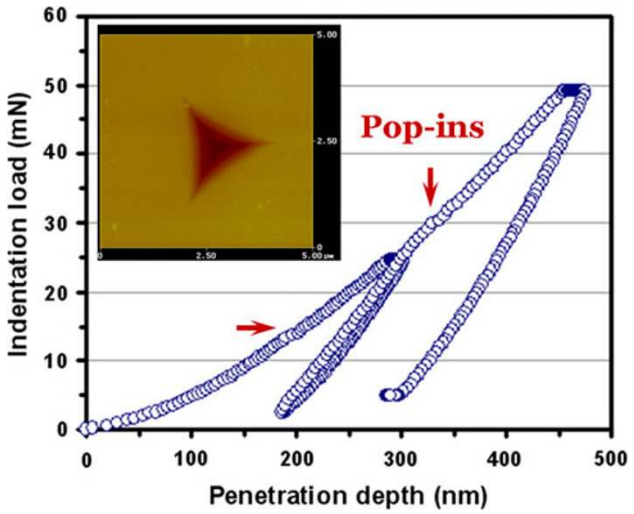

Fig. 3 AFM image (*inset*) of a Berkovich indentation on AlN thin film obtained at an indentation load of 50 mN and, the multiple "pop-ins" also displayed in the load–displacement curve

The typical results obtained with an indentation load of 50 mN and penetration depth of 500 nm, as shown in Fig. 3. Similar features of multiple pop-ins are evident, although the resolution is much reduced because of larger indentation load. In fact, the multiple pop-ins are observable over such a wide range of indentation load and the penetration depth indicates the close relations to the plastic deformation of AlN thin film. Also, a closer look at the loading curves displayed in Figs. 1 and 3 reveals that the multiple pop-ins do not exactly coincide at the same indenter penetration depths. Since each curve is associated with different stress rates depending on the maximum indentation load, suggesting that the first pop-in event is not thermally activated. Instead, these phenomena are usually attributed to dislocation nucleation or/and propagation during loading as have been investigated in a wide variety of materials [21–23], or micro-cracking [24, 25]. Moreover, the reverse discontinuities during unloading curve, the so-called "pop-out" event, commonly observed in Si and has been attributed to pressure-induced phase transformation [26–28], is not observed here. Therefore, it is clear that the first pop-in event may reflect the transition from perfectly elastic to plastic deformation, that is, it is the onset of plasticity in AlN thin film. The corresponding shear stress under the Berkovich indenter at an indentation load, P^*, where the load–displacement discontinuity occurs, can be determined by using the following relation [29]:

$$\tau_{\max} = 0.31\left(\frac{6P^*E^2}{\pi^3R^2}\right)^{0.33} \quad (4)$$

where R is the radius of the tip of the indenter, and E is defined in terms of Young's moduli and Poisson's ratios of the diamond indenter and thin film. The maximum shear stress, $\tau_{\max}$, of AlN thin film is 7.35 GPa.

The inset of Fig. 3 shows the typical AFM image for an indented surface obtained with an indentation load of 50 mN. There is no evidence of either dislocation activity or crack formation in the area of the indented surface. Therefore, if the dislocation nucleation and subsequent propagation are indeed the primary mechanism for the observed multiple pop-ins, it should prevail underneath the indented surface. It is also interesting to check if there is any pressure-induced phase transformation involved.

To further clarify the nanoindentation-induced deformation, micrographs of plastic zones (bright-field XTEM observations) with the selected area diffraction (SAD) pattern from Berkovich indentation in AlN thin film are displayed in Fig. 4. In Fig. 4, the width of the indented area was $\sim$3 μm and its depth was a maximum of $\sim$2 μm at the center of the indent. Indentation to a load of 50 mN, increased the local compressive plastic strain in AlN thin film to $\sim$45%, resulting in bending at the interface together with dislocations accumulation and slip bands oriented at $\sim$60° to the surface in AlN thin film significantly. In addition, at 50 mN sufficient indentation load is transferred through AlN thin film to cause deformation in GaN thin film. Below the indented zone, the extent of plastic deformation in GaN thin film increases. It can be found that, the slip bands are aligning parallel to the {0001} basal planes and the dislocations gliding along the $\{10\bar{1}1\}$ pyramidal planes intersected and then distorted each of basal slip bands along the basal planes. Details of the nanoindentation-induced deformation mechanisms in GaN thin films can be found elsewhere [17, 30, 31].

Furthermore, to further confirm whether phase transformation occurred beneath the indent, SAD analysis of the deformed area (region I) was shown. We do not observe any halo rings in SAD result; therefore, we can say that AlN thin film did not undergo the amorphization in Berkovich nanoindentation. It can also be expected that the distortion of diffraction spots is more significantly than the pristine one (not shown here), demonstrating a nanoindentation load effect on the plastic deformation intensity. According to the above-mentioned results, we can conclude that although significant plastic deformation occurs in AlN thin film beneath the Berkovich indenter, no phase transformation is induced.

Conclusion

To summarize, a combination of nanoindentation, FIB, and TEM techniques was used to investigate the contact-induced structural deformation behaviors in the AlN thin films.

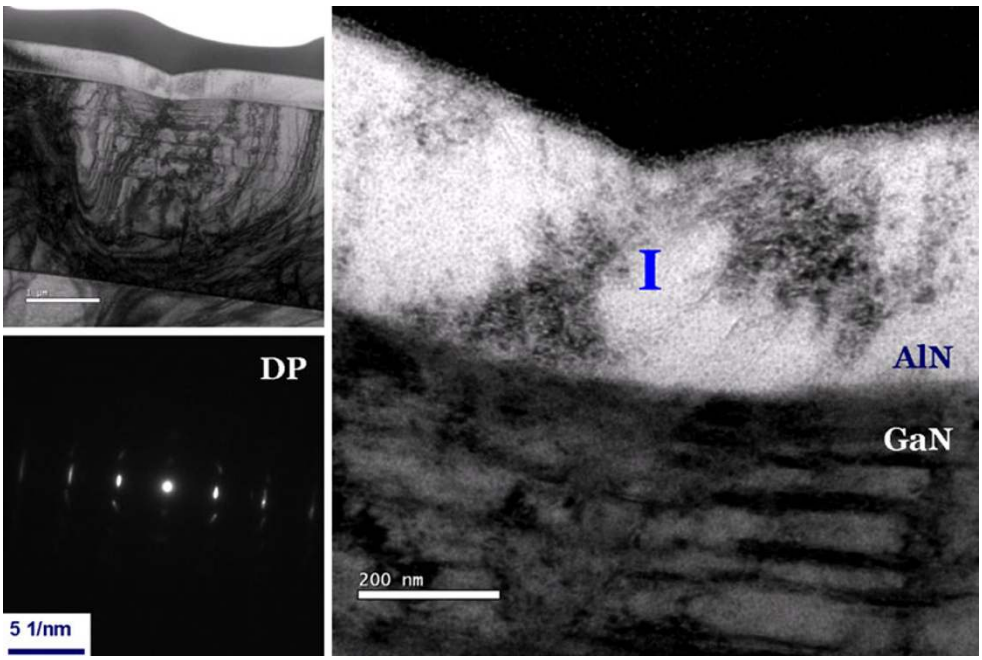

Fig. 4 Bright-field XTEM image of AlN thin film subjected to an indentation load of 50 mN. And, selected area diffraction pattern results of sample underneath the Berkovich indent from the region (I): indented AlN thin film. A close-up view of XTEM image of the deformed zone of AlN thin film, showing that several slip bands are along the $\sim 60^{\circ}$ pyramidal planes

The load–displacement curves show the multiple "pop-ins" during nanoindentation loading. No evidence of either nanoindentation-induced phase transformation or formation of micro-cracking is observed in AlN thin film by AFM and XTEM. Also, XTEM observation revealed that the primary deformation mechanism in GaN thin film is via propagation of dislocations on both basal and pyramidal planes. Finally, as displayed in SAD result, the distortion of diffraction spots, however, does indicate severe deformation of indented AlN thin film resulting from the nanoindentation load. The CSM technique was used to determine the hardness and Young's modulus of AlN thin films. Furthermore, analysis of the load–displacement data reveals that the values of hardness and Young's modulus of AlN thin films are 22 and 332 GPa, respectively.

Acknowledgments This study was partially supported by the National Science Council of Taiwan, under Grant No.: NSC97-2112-M-214-002-MY2. Author likes to thank Dr. Y.-S. Lai and Dr. P.-F. Yang for their technical support (Central Product Solutions, Advanced Semiconductor Engineering, Taiwan), and Dr. M.-R. Chen and Prof. H.-L. Kao (Department of Electronic Engineering, Chung Yuan Christian University, Taiwan) for their support in AlN thin films.

References

1. J. Li, Z.Y. Fan, R. Dahal, M.L. Nakarmi, J.Y. Lin, H.X. Jiang, Appl. Phys. Lett. **89**, 213510 (2006)
2. Y. Taniyasu, M. Kasu, T. Makimoto, Nature **441**, 325 (2006)
3. A.T. Sowers, J.A. Christman, M.D. Bremser, B.L. Ward, R.F. Davis, R.J. Nemanich, Appl. Phys. Lett. **71**, 2289 (1997)
4. V. Mortet, O. Elmazria, M. Nesladek, M.B. Assouar, G. Vanhoyland, J. D'Haen, M. D'Olieslaeger, P. Alnot, Appl. Phys. Lett. **81**, 1720 (2002)
5. T. Matsutani, M. Kiuchi, K. Shirouzu, A. Yoshioka, R. Shimizu, S. Takahashi, Solid State Phenom. **107**, 43 (2005)
6. X.D. Li, H. Gao, C.J. Murphy, L. Gou, Nano Lett. **4**, 1903 (2004)
7. X. Tao, X. Wang, X.D. Li, Nano Lett. **7**, 3172 (2007)
8. X. Tao, X.D. Li, Nano Lett. **8**, 505 (1008)
9. S.R. Jian, J.S.C. Jang, Y.S. Lai, P.Y. Yang, C.S. Yang, H.C. Wen, C.H. Tsai, Mater. Chem. Phys. **109**, 360 (2008)
10. S.R. Jian, I.J. Teng, P.F. Yang, Y.S. Lai, J.M. Lu, J.G. Chang, S.P. Ju, Nanoscale Res. Lett. **3**, 186 (2008)
11. S.R. Jian, J.S.C. Jang, G.J. Chen, H.G. Chen, Y.T. Chen, J. Alloys Compd. **479**, 348 (2009)
12. S.R. Jian, G.J. Chen, J.S.C. Jang, Y.S. Lai, J. Alloys Compd. **494**, 219 (2010)
13. W.C. Oliver, G.M. Pharr, J. Mater. Res. **7**, 1564 (1992)
14. T.Y. Tsui, G.M. Pharr, J. Mater. Res. **14**, 292 (1999)
15. X.D. Li, B. Bhushan, Mater. Charact. **48**, 11 (2002)
16. A. Mujica, A. Rubio, A. Muñoz, R.J. Needs, Rev. Mod. Phys. **75**, 863 (2003)
17. C.H. Chien, S.R. Jian, C.T. Wang, J.Y. Juang, J.C. Huang, Y.S. Lai, J. Phys. D Appl. Phys. **40**, 3985 (2007)
18. A.P. Zhang, G.T. Dang, F. Pen, H. Cho, K.P. Lee, S.J. Pearton, J.I. Chyi, T.E. Nee, C.M. Lee, C.C. Chuo, IEEE Trans. Electron Devices **48**, 407 (2001)

19. J.D. Wu, W.C. Chien, H.L. Kao, J.I. Chyi, C.H. Hsu, Phys. Stat. Sol. A **204**, 3349 (2007)
20. J.E. Bradby, J.S. Williams, M.V. Swain, J. Mater. Res. **19**, 380 (2004)
21. S.O. Kucheyev, J.E. Bradby, J.S. Williams, C. Jagadish, M.V. Swain, Appl. Phys. Lett. **80**, 956 (2002)
22. T. Scholz, K.K. McLaughlin, F. Giuliani, W.J. Clegg, F.J. Espinoza-Beltrán, M.V. Swain, G.A. Schneider, Appl. Phys. Lett. **91**, 062903 (2007)
23. S.R. Jian, Appl. Surf. Sci. **254**, 6749 (2008)
24. S.J. Bull, J. Phys. D Appl. Phys. **38**, R393 (2005)
25. S.R. Jian, J.S.C. Jang, J. Alloys Compd. **482**, 498 (2009)
26. J.E. Bradby, J.S. Williams, J. Wong-Leung, M.V. Swain, P. Munroe, Appl. Phys. Lett. **77**, 3749 (2000)
27. S. Ruffell, J.E. Bradby, J.S. Williams, D. Munoz-Paniagua, S. Tadayyon, L.L. Coatsworth, P.R. Norton, Nanotechnology **20**, 135603 (2009)
28. S.R. Jian, G.J. Chen, J.Y. Juang, Curr. Opin. Solid State Mater. Sci. doi:10.1016/j.cossms.2009.11.002
29. K.L. Johnson, *Contact Mechanics* (Cambridge University Press, Cambridge, UK, 1985)
30. J.E. Bradby, J.S. Williams, J. Wong-Leung, S.O. Kucheyev, M.V. Swain, P. Munroe, Phil. Mag. A **82**, 1931 (2002)
31. J.E. Bradby, S.O. Kucheyev, J.S. Williams, J. Wong-Leung, M.V. Swain, P. Munroe, G. Li, M.R. Phillips, Appl. Phys. Lett. **80**, 383 (2002)